www.lpr-journal.org Vol. 7 No. 5 September 2013

LASER & PHOTONICS REVIEWS

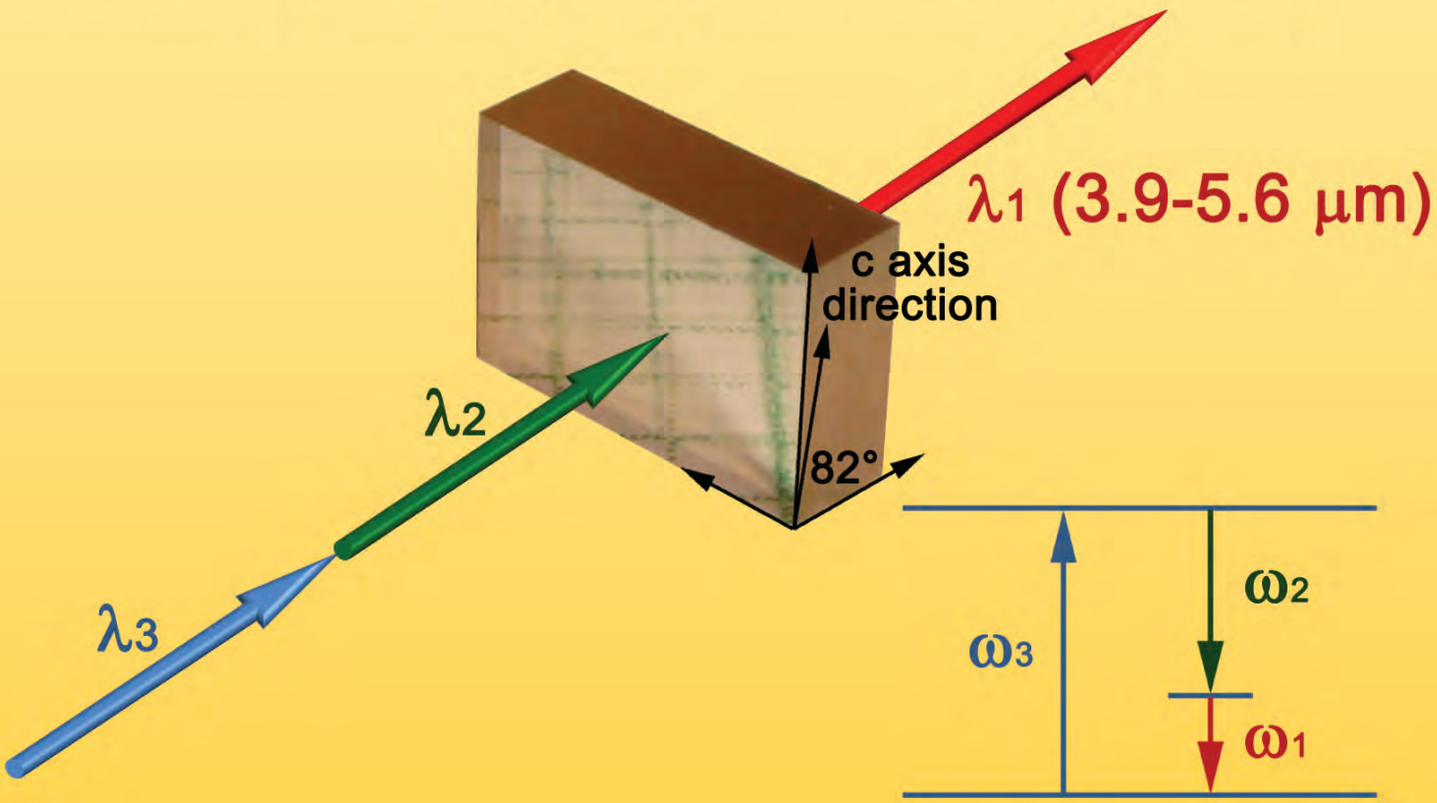

4H-SiC: a new nonlinear material for midinfrared lasers

Nonlinear optical (NLO) frequency conversion is commonly used for generating midinfrared (MIR) lasers that offer light sources for a variety of applications. However, the low laser damage thresholds of NLO crystals used so far seriously limit the output power of MIR lasers. **Shunchong Wang et al. (pp. 831-838)** demonstrate a new nonlinear material 4H-SiC for producing midinfrared laser. Broadband midinfrared laser ranging from 3.90 to 5.60 μm is generated in 4H-SiC by phase-matched difference-frequency generation for the first time. The results may open a door to practically utilize wide bandgap semiconductors with high laser damage thresholds as nonlinear optical materials for high power output of midinfrared lasers.

WILEY-VCH

Laser Photonics Rev. **7,** No. 5, 831–838 (2013) / **DOI** 10.1002/lpor.201300068

LASER & PHOTONICS REVIEWS

Abstract Nonlinear optical (NLO) frequency conversion is commonly used for generating midinfrared (MIR) lasers that offer light sources for a variety of applications. However, the low laser damage thresholds of NLO crystals used so far seriously limit the output power of MIR lasers. Here, a new nonlinear material 4H-SiC is demonstrated for producing MIR laser. Broadband MIR radiation ranging from 3.90 to 5.60 μm is generated in 4H-SiC by phase-matched difference-frequency generation for the first time. The results may open a door to practically utilize wide-bandgap semiconductors with high laser damage thresholds as NLO materials for high power output of MIR lasers.

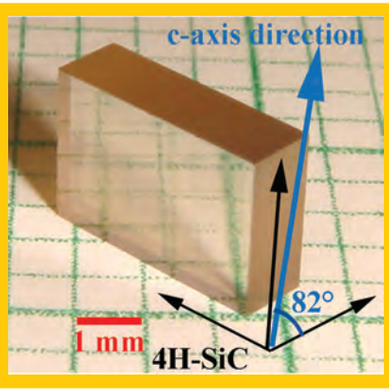

ORIGINAL PAPER

4H-SiC: a new nonlinear material for midinfrared lasers

Shunchong Wang[1], Minjie Zhan[2], Gang Wang[1,*], Hongwen Xuan[2], Wei Zhang[2], Chunjun Liu[1], Chunhua Xu[1], Yu Liu[1], Zhiyi Wei[2], and Xiaolong Chen[1,*]

1. Introduction

Midinfrared (MIR) lasers offer desired light sources for a variety of applications, such as molecular identification, industrial and environmental monitoring, medical diagnostics, rapid detection of explosives, free-space communication, and thermal imaging. Lead-salt laser diodes [1] and quantum cascade lasers [2] are commonly used to generate laser light in this wavelength range, but both suffer from shortcomings. The former is often hindered in applications by requiring low working temperatures [3] and the latter by outputting low power and astigmatic beams [4, 5]. On the other hand, generation of lasers with wavelengths longer than 3 μm based on solid-state lasers is limited by the multiphonon relaxation process in gain medium at room temperature [6]. Over the past decades, frequency conversion through using nonlinear optical (NLO) crystals has found more and more practical applications in producing MIR lasers. The NLO crystals used so far include $LiNbO_3$ [7], $AgGaS_2$ [8], $AgGaSe_2$ [9], $ZnGeP_2$ [10], GaSe [11] etc. The key to this technique lies in the NLO crystals as they usually possess high NLO coefficients but low damage thresholds ($<$100 MW cm^{-2}) [9, 12–15]. It is the low damage threshold that limits outputting high-power MIR lasers and hence cannot meet the increasing power demand in various applications. Therefore, exploring new NLO crystals with higher damage thresholds has been a pressing and important issue in this field.

Although the damage mechanism of NLO crystals by lasers has not been fully understood [16–18], it is generally believed that weak covalent bonds or high ionicity within compounds are the main reasons responsible for low damage threshold. The NLO crystals like sulfides, selenides, and oxides with alkali metals are not good candidates to this end. Silicon carbides (SiCs), as wide-bandgap semiconductors, are well known for their extensive applications in high-power, high-frequency, and high-temperature devices [19] due to their wide bandgap (2.3–3.2 eV) [20], high thermal conductivity (about 480 W m^{-1} K^{-1}) [21], and high bond energy (about 5 eV/bond) [22]. Si atoms and C atoms are tetrahedrally bonded to each other and stack in different ways to form many polytypes. Among them, 6H-SiC and 4H-SiC are the most common ones. Their structures are shown in Figs. 1a and b, both crystallizing in 6 mm point group. Symmetry 6 mm means that they are uniaxial crystals and exhibit the second-order NLO effect. If the birefringence is proper, phase matching could be attainable by taking appropriate polarizations and propagation directions of the light travelling in SiC crystals. The refractive indices of 6H-SiC and 4H-SiC were previously investigated in the visible and near-infrared region [23–25]. Calculations based on these data predicted that phase-matched second-harmonic generation (SHG) [24] or optical parametric oscillator (OPO) [26] were probable in the MIR region in 6H-SiC. Up to now, however, experimental realization of MIR radiation in SiC has never been reported to the best of our knowledge [27–33].

In this study, we demonstrate a MIR laser output tunable from 3.90 to 5.60 μm by phase-matched difference-frequency generation (DFG) in 4H-SiC for the first time.

[1] Research & Development Center for Functional Crystals, Beijing National Laboratory for Condensed Matter Physics, Institute of Physics, Chinese Academy of Sciences, Beijing 100190, China
[2] Key Laboratory of Optical Physics, Beijing National Laboratory for Condensed Matter Physics, Institute of Physics, Chinese Academy of Sciences, Beijing 100190, China
*Corresponding authors: e-mail: gangwang@iphy.ac.cn; chenx29@iphy.ac.cn

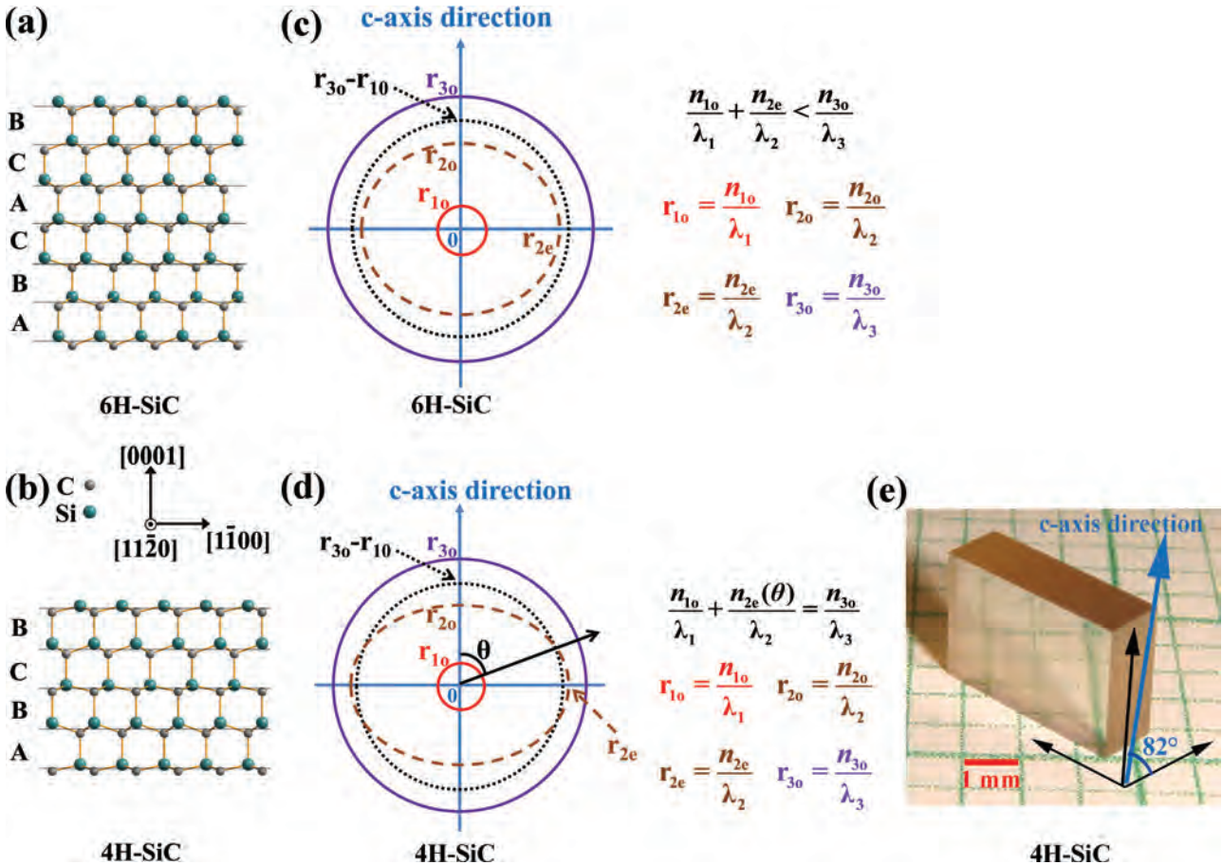

Figure 1 (a) and (b) Schematic cross-sectional depictions of 6H-SiC and 4H-SiC structures. The repeated stacking sequences of 6H-SiC and 4H-SiC along [0001] direction are ABCACB and ABCB, respectively. (c) and (d) The schematic of principle of type II phase matching for 6H-SiC and 4H-SiC, respectively. n_{1o}, n_{2o}, and n_{3o} are the ordinary refractive indices for wavelengths λ_1, λ_2, and λ_3, respectively. n_{2e} is the extraordinary refractive index for wavelength λ_2. The plotting is based on the nonlinear process ($\frac{1}{\lambda_1}+\frac{1}{\lambda_2}=\frac{1}{\lambda_3}$) with $\lambda_1 = 3.90$ μm, $\lambda_2 = 0.928$ μm, and $\lambda_3 = 0.75$ μm. The refractive indices are obtained from Eqs. (1)–(4) in this work. The difference between r_{2o} and r_{2e} is plotted much larger than the real value for clarity. The phase-matching condition is satisfied at the intersections of the dashed and dotted surfaces in 4H-SiC with $\theta = 82^\circ$, while it is impossible to achieve the phase-matching condition for 6H-SiC. (e) The 4H-SiC crystal for DFG experiment cutting at an angle of 82° with respect to the optical axis (*c*-axis).

The phase matching can be realized on semi-insulating (SI) 4H-SiC crystals with phase-matching angle (PMA) from 74.6–89.4° with available input light based on our re-evaluation of the refractive indices from visible light extending to the MIR light range. We also verify phase matching is impossible in 6H-SiC. The results may open the door to practically utilizing wide-bandgap semiconductors with high damage thresholds as NLO materials for high power output of MIR lasers.

2. Experimental method

2-inch SI 6H-SiC and 3 inch SI 4H-SiC (0001) wafers (TankeBlue, Beijing) with thicknesses of 353 and 379 μm respectively, were selected for transmission measurements using Fourier transform infrared spectrometers (TU-1901, FTS-60V, and FTS-6000). 2-inch SI 6H-SiC with a thickness of 0.4 mm and 3-inch SI 4H-SiC with a thickness of 0.6 mm (TankeBlue, Beijing) were cut into pieces of 20 $\times$ 20 mm^2 for the laser damage threshold test using a Q-switched Nd:YAG laser. The Nd:YAG laser was operated in the TEM_{00} mode with 5 ns pulse width at 1064 nm. The laser beam was focused on the crystal surface with a diameter of 150 μm. The test mode is 1-on-1 according to the International Standard Organization 11254–1 [34]. SI 6H-SiC and 4H-SiC boules (TankeBlue, Beijing) were cut into triangular prisms with apex angles of 18.34° and 16.69°, respectively. The heights of the 6H-SiC and 4H-SiC prisms (along the *c*-axis) were about 10 mm and 8 mm, respectively. The refractive indices were measured as functions of wavelength (0.4047–2.325 μm) by the method of minimum deviation (SpectroMaster UV-VIS-IR). The ordinary refractive indices of 4H-SiC at wavelengths ranging from 3.00 to 5.00 μm were measured by the arbitrary ray deviation method [35].

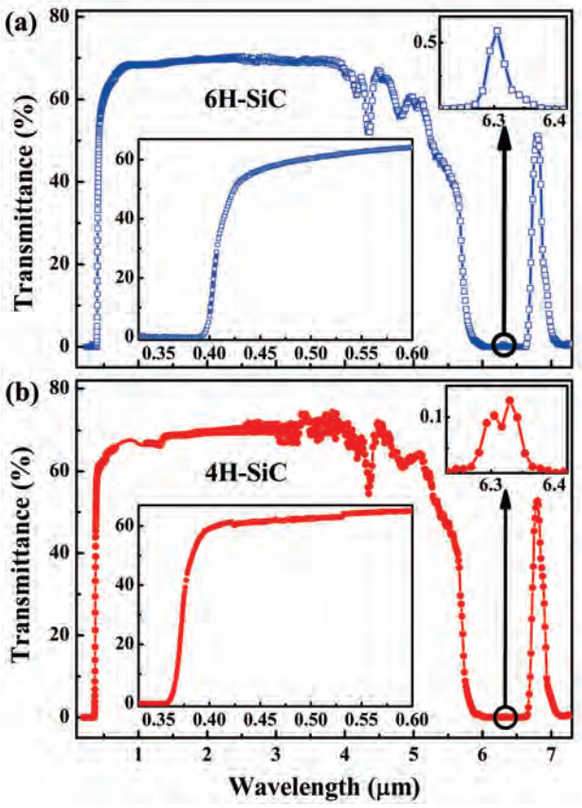

Figure 2 (a) The optical transmittance spectrum of SI 6H-SiC (0001) wafer with thickness of 353 μm and (b) the optical transmittance spectrum of SI 4H-SiC (0001) wafer with thickness of 379 μm.

For the DFG experiment, the pump laser source is composed of a 25-fs chirped-pulse amplified Ti:sapphire system (Femtolasers Femtopower Pro) and a gas-filled (0.2 MPa neon) hollow fiber. A set of chirped mirrors was used to compensate the dispersion caused by the neon gas. More information about the laser system can be found in the literature [36]. The spectrum of the input light was measured by a spectrometer (Avaspec-2048FT, Avantes). A Ge filter was used to block the input light, transmitting only the MIR beam. The generated MIR beam was collimated into a monochromator (Zolix Omni-λ, 150-DZ2) and detected by a HgCdTeZn detector (Vigo System S. A., PCI-3TE-10.6) together with a lock-in amplifier system (SR830, Stanford). The average MIR output power was measured by an EPM2000 Powermeter (Coherent, Inc.) and an energy sensor (J-10MB-LE).

3. Results and discussion

We first examined the optical properties of transparent SiC crystals. The optical transmittance spectra of SI 6H-SiC and 4H-SiC wafers with corresponding thicknesses of 353 and 379 μm are shown in Fig. 2. The band-edge absorptions start from around 0.40 and 0.37 μm for 6H-SiC and 4H-SiC, respectively, as shown in the lower insets of Fig. 2. In the visible and MIR regions, the transmittances of both 6H-SiC and 4H-SiC are greater than 50%, then decrease rapidly at a wavelength around 5.60 μm. It is noted that there are transmittance windows centered at around 6.30 and 6.80 μm for 6H-SiC and 4H-SiC. Their laser damage thresholds were tested and no damage was observed up to a power density of 3.0 GW cm^{-2}, more than one order larger than the NLO crystals used in the MIR region.

The refractive indices of SiC in the MIR range formerly were obtained by extrapolating the dispersion equations based on the data measured in the visible and near-infrared regions [24]. These data deviate markedly from real values as we never observed phase matching based on these refractive indices. The refractive indices and the birefringence are the most important parameters that determine if phase matching can be realized. Here we remeasured the index data from the visible to the MIR region by using deviation of angle through a prism. The measured ordinary (n_o) and extraordinary (n_e) refractive indices of 6H-SiC and 4H-SiC, as listed in Table S1 in the Supporting Information [37], are fitted to the Sellmeier equations by using the least squares method. The average deviation between the experimental refractive indices and the calculated data is within 2.0 $\times$ 10^{-4}. The obtained dispersion equations are as follows:

$$n^2_{o\text{-}6H}(\lambda) = 6.57232 + \frac{0.1401}{\lambda^2 - 0.03178} - 0.02153\lambda^2 \quad (1)$$

$$n^2_{e\text{-}6H}(\lambda) = 6.7452 + \frac{0.15352}{\lambda^2 - 0.03597} - 0.02249\lambda^2 \quad (2)$$

$$n^2_{o\text{-}4H}(\lambda) = 1 + \frac{0.20075\lambda^2}{\lambda^2 + 12.07224} + \frac{5.54861\lambda^2}{\lambda^2 - 0.02641} + \frac{35.65066\lambda^2}{\lambda^2 - 1268.24708} \quad (3)$$

$$n^2_{e\text{-}4H}(\lambda) = 6.79485 + \frac{0.15558}{\lambda^2 - 0.03535} - 0.02296\lambda^2, \quad (4)$$

where the wavelength λ is in micrometers. As shown in Figs. 3a–c, the refractive indices of 6H-SiC and 4H-SiC in the visible region are consistent with those given in Ref. [23] and [24], but deviate a lot from those in Ref. [26]. In the MIR region, our data are much smaller than those obtained by extrapolating the dispersion equations, and the disagreements increase with increasing wavelength [23,24]. We will verify that the predictions on phased-matched SHG and OPO in 6H-SiC based on the new refractive indices are out of the question, explaining why they have been never experimentally observed. On the other hand, phase-matched DFG and OPO are possible in 4H-SiC, though

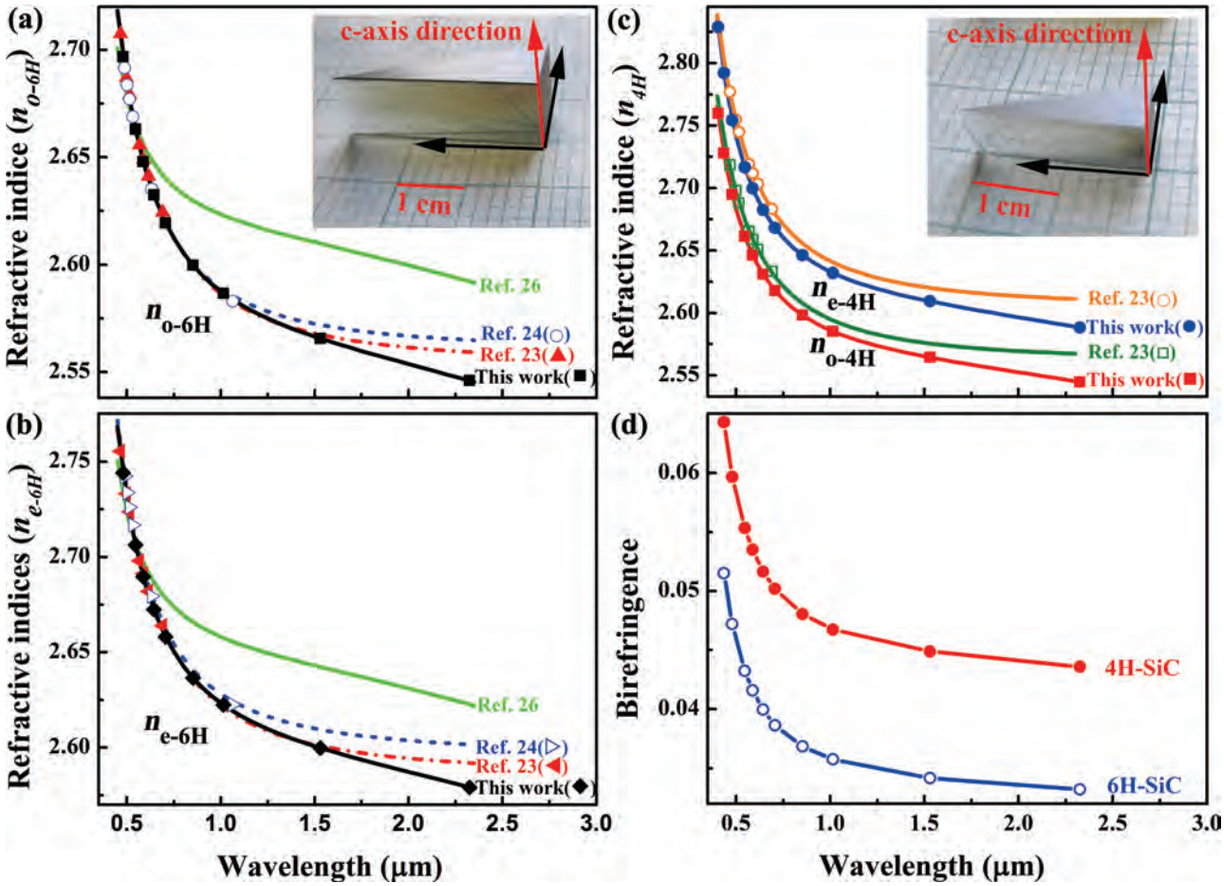

Figure 3 (a)–(c) Dispersion of ordinary refractive indices of SI 6H-SiC, extraordinary refractive indices of SI 6H-SiC, and refractive indices of SI 4H-SiC, respectively. Previous results are also presented for comparison. Data points are experimental values of the refractive indices. Lines are calculated from the Sellmeier equations. The insets in (a) and (c) are 6H-SiC and 4H-SiC prisms used in this work, respectively. (d) Wavelength-dependent birefringence for SI 6H-SiC and 4H-SiC measured by this work. The line is a guide to the eye.

phase-matched SHG is not achievable over the transparency range 0.37–6.00 μm.

For 6H-SiC and 4H-SiC with 6 mm point group symmetry, type I phase matching, where the two low-frequency waves have the same polarization, is not achievable due to the zero effective second-order nonlinear coefficient ($\chi^{(2)}_{\text{eff}}$) according to Kleinman symmetry conditions [38], whereas type II phase matching, in which the two low frequency waves have orthogonal polarizations, is possible ($\chi^{(2)}_{\text{eff}} = \chi^{(2)}_{\text{xxz}} \sin\theta$, θ is the PMA) [24, 27]. The principle of type II phase matching for the positive uniaxial 6H-SiC and 4H-SiC is depicted in Figs. 1c and d. In a nonlinear process involving three waves with wavelengths λ_1, λ_2, and λ_3 (assuming that $\lambda_3 < \lambda_2 \le \lambda_1$) related by

$$\frac{1}{\lambda_1} + \frac{1}{\lambda_2} = \frac{1}{\lambda_3} \tag{5}$$

type II phase matching occurs when $\frac{n_{1e}(\theta)}{\lambda_1} + \frac{n_{2o}}{\lambda_2} = \frac{n_{3o}}{\lambda_3}$ (e+o→o) or $\frac{n_{1o}}{\lambda_1} + \frac{n_{2e}(\theta)}{\lambda_2} = \frac{n_{3o}}{\lambda_3}$ (o+e→o), where $n_{1e}(\theta) = (\frac{\sin^2\theta}{n_{1e}^2} + \frac{\cos^2\theta}{n_{1o}^2})^{-\frac{1}{2}}$, $n_{2e}(\theta) = (\frac{\sin^2\theta}{n_{2e}^2} + \frac{\cos^2\theta}{n_{2o}^2})^{-\frac{1}{2}}$, $n_{1e}(\theta)$ and $n_{2e}(\theta)$ are the refractive indices for the extraordinary rays propagating at an angle of θ with respect to the optical axis at wavelengths λ_1 and λ_2, respectively, n_{1e} and n_{2e} are the principal values of the extraordinary refractive indices at wavelengths λ_1 and λ_2, respectively, n_{1o}, n_{2o}, and n_{3o} are the ordinary refractive indices at wavelengths λ_1, λ_2, and λ_3, respectively.

The derived equations for type II PMAs are as follows:

$$\sin^2\theta = \frac{n_{1e}^2\left[\left(\frac{n_{3o}}{\lambda_3} - \frac{n_{2o}}{\lambda_2}\right)^2 - \left(\frac{n_{1o}}{\lambda_1}\right)^2\right]}{\left(n_{1e}^2 - n_{1o}^2\right)\left(\frac{n_{3o}}{\lambda_3} - \frac{n_{2o}}{\lambda_2}\right)^2} \quad (e + o \to o) \tag{6}$$

$$\sin^2\theta = \frac{n_{2e}^2\left[\left(\frac{n_{3o}}{\lambda_3} - \frac{n_{1o}}{\lambda_1}\right)^2 - \left(\frac{n_{2o}}{\lambda_2}\right)^2\right]}{\left(n_{2e}^2 - n_{2o}^2\right)\left(\frac{n_{3o}}{\lambda_3} - \frac{n_{1o}}{\lambda_1}\right)^2} \quad (o + e \to o) \tag{7}$$

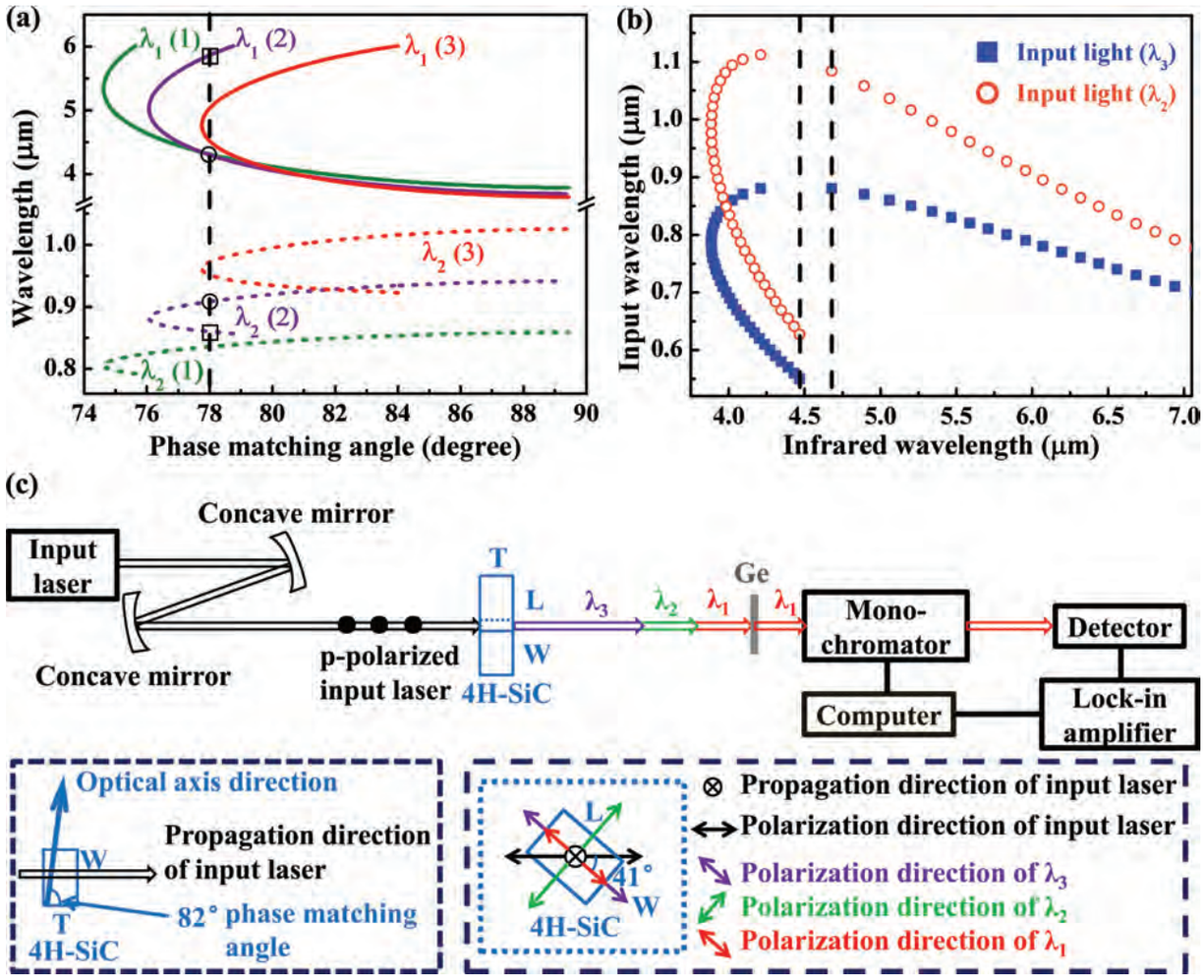

Figure 4 (a) Calculated PMAs for SI 4H-SiC DFG at three fixed wavelengths of $\lambda_3 = 0.70$ μm (1), 0.75 μm (2), 0.8 μm (3), respectively. The generated infrared light (λ_1) is continuously tunable from 3.64 to 6.00 μm. The other input light (λ_2) from 0.79 to 1.02 μm is required and the PMAs lie in 74.6–89.4°. For $\lambda_3 = 0.75$ μm under a PMA at 78°, the desired output light is set at 5.86 μm, then another input light at 0.86 μm is needed as indicated by the square marks on the dashed line. Alternatively, when $\lambda_1 = 4.27$ μm, then $\lambda_2 = 0.91$ μm as indicated by the circular marks. (b) Calculated output wavelengths (λ_1) for 4H-SiC DFG as a function of input wavelengths for $\theta = 82°$. The ranges of λ_3 and λ_2 are from 0.55 to 0.88 μm and 0.63 to 1.10 μm, respectively. A small light gap from 4.50 to 4.70 μm cannot be output when PMA is at 82°. (c) Schematic of the experimental setup for DFG in 4H-SiC. *T*, *L*, and *W* are thickness, length and width directions of 4H-SiC, respectively.

Inserting the refractive indices according to Eqs. (1) and (2) into Eqs. (6) and (7), we found that Eqs. (6) and (7) cannot be satisfied over the entire transparency range (0.40–6.00 μm) for 6H-SiC.

4H-SiC has a larger birefringence than that of 6H-SiC (see Fig. 3d) and the calculations based on Eqs. (3), (4), (6), and (7) indicate that phase matching can be satisfied (Eq. (7) for frequency downconversion into the MIR region (λ_1) at wavelengths larger than 3.60 μm. For frequency conversion in 4H-SiC, DFG is preferred over OPO and optical parametric amplifiers for its straightforward geometries and no oscillation threshold. Considering the light transmittance spectrum in the MIR range for 4H-SiC, we hope to output 3.60 to 6.00 μm light, λ_1, by the DFG technique. If an input light, λ_3, at a range from 0.50 μm to 0.80 μm, then another input light, λ_2, is needed to be at 0.55 μm to 1.03 μm, according to Eq. (5) under the phase-matching condition. Figure 4a shows the calculated PMAs in 4H-SiC for DFG at three fixed input wavelengths of $\lambda_3 = 0.70$ μm, 0.75 μm, and 0.80 μm, respectively. The generated infrared light (λ_1) is continuously tunable from 3.64 to 6.00 μm, while another input light (λ_2) from 0.79 to 1.02 μm is required. In so doing, the PMAs lie in 74.6–89.4°. Take $\lambda_3 = 0.75$ μm under a PMA at 78° as an example. In this case, if the desired output light is set at 5.86 μm, then another input light at 0.86 μm is needed, as indicated by the square marks on the dashed

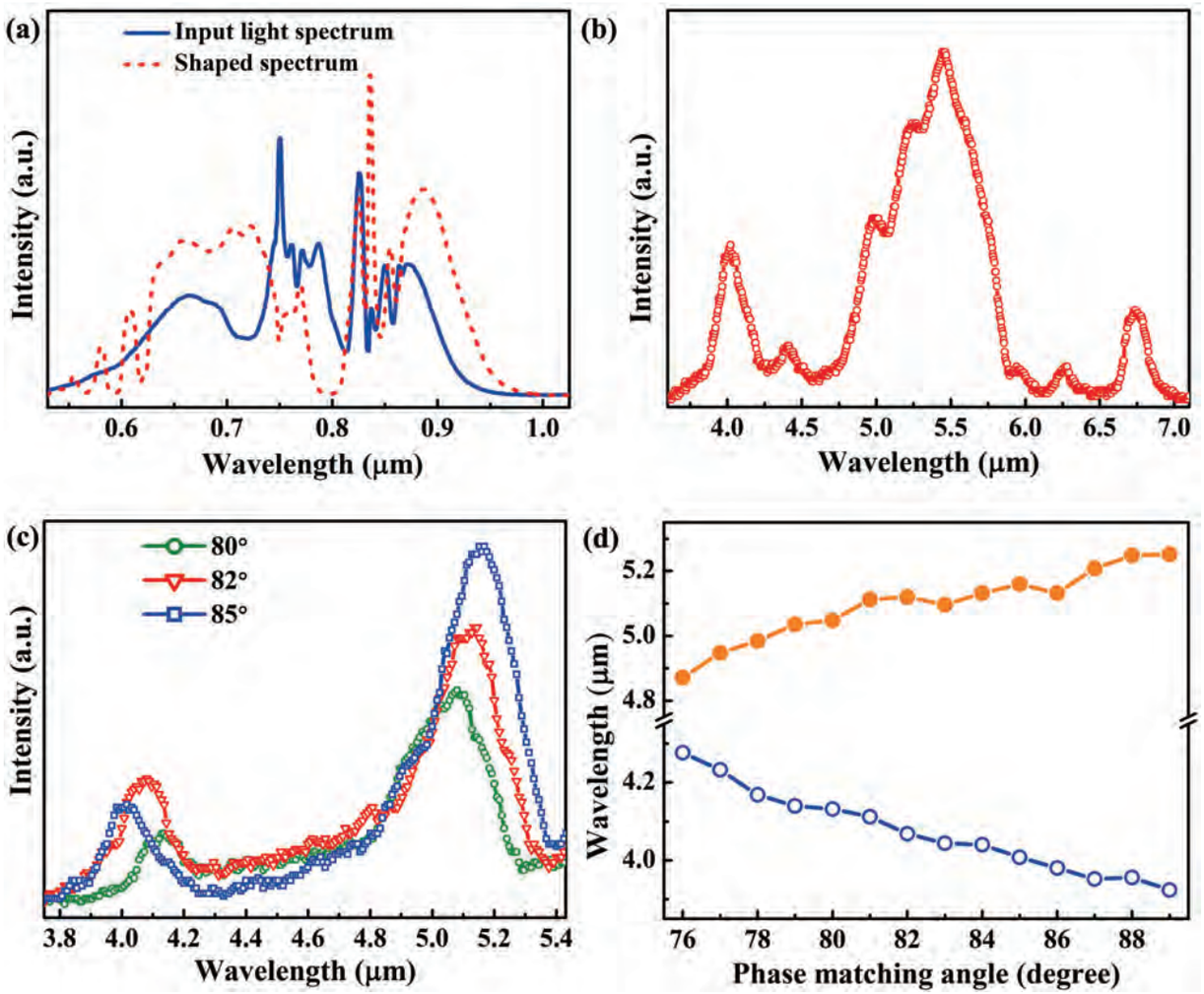

Figure 5 (a) The spectrum of the femtosecond pump laser output from chirped-pulse amplified Ti:sapphire laser system. The shaped spectrum with two mirrors is also presented. (b) The broadband MIR radiation generated by DFG in 4H-SiC for $\theta = 82^\circ$. (c) The output spectra with respect to PMAs of 80°, 82°, and 85°, respectively. (d) The output wavelength tuning of two dominant peaks in 4H-SiC DFG under various PMAs. The line is a guide to the eye.

line shown in Fig. 4a. Alternatively, if $\lambda_1 = 4.27$ μm, then $\lambda_2 = 0.91$ μm, as indicated by the circular marks. On the other hand, for a given PMA, we can calculate the whole input light ranges of λ_2 and λ_3 that guarantee the output light λ_1 in the MIR range. Figure 4b shows the ranges of λ_2 and λ_3 corresponding to λ_1 from 3.90 to 7.00 μm under a PMA of 82°. We note that there exists a small light gap from 4.50 to 4.70 μm that cannot be output at this PMA, which is limited by the cut-off edge in the shorter wavelengths of the pumping laser.

The experimental setup of DFG is schematically illustrated in Fig. 4c. The broadband 5-fs laser pulses generated from a chirped-pulse amplified Ti:sapphire laser at 1 kHz repetition rate were used as the input light source. Phase matching is expected to be achieved based on the interaction between specific wavelengths contained in the input broadband spectrum from 0.55 μm to 0.97 μm (Fig. 5a). Our setup is much simpler in performing DFG experiment, which usually requires mixing either two synchronized ultrafast lasers [39] or the signal and idler lights generated by the optical parametric process [40]. The SI 4H-SiC crystal used in the DFG was 7 (length) × 5 (width) × 2.62 (thickness) mm^3 and cut at an angle of 82° with respect to the optical axis (see Fig. 1e). Both end surfaces were uncoated. For type II phase matching, the input light was split into ordinary (λ_3) and extraordinary (λ_2) components in 4H-SiC by setting the normal direction of the principal plane of 4H-SiC at an angle of α ($0^\circ < \alpha < 90^\circ$) with respect to the polarization direction of the incident beam. Here, α was fixed at about 41° at which the output intensity was around its maximum. Figure 5b displays the power of the generated MIR output, recorded from 3.60 μm to 7.00 μm with a step size of 4 nm. In this process, each output light at a certain wavelength is converted by a pair of light

beams λ_2 and λ_3 with specific wavelengths according to Fig. 4b. Maximum power output occurs at 5.45 μm and an average power of 0.2 mW was obtained for an input power of 430 mW. The low output power at wavelengths ranging from 4.50 to 4.70 μm is due to the loss of phase matching (see Fig. 4b), the reduced output power at wavelengths longer than 5.60 μm resulting from the strong absorption by 4H-SiC (see Fig. 2b). The wavelength at which the maximum power is output can be adjusted by changing the PMA or the relative intensity of input lights.

Furthermore, we studied the PMA-dependent output by varying the angles between the incident light and the surface normal of 4H-SiC in order to investigate the tunability of the output. We attenuated the incident spectrum between 0.78 and 0.81 μm (see Fig. 5a) by using two mirrors to suppress the undesired input lights. The generated MIR radiations under three different PMAs are shown in Fig. 5c. It is noted that two dominant output peaks shift effectively from 4.13 (5.05) μm to 4.00 (5.16) μm with increasing PMAs. Figure 5d shows the shift of output wavelength for two dominant peaks in 4H-SiC DFG under various PMAs. Two tunable domains of output lights, 3.92–4.28 μm, and 4.87–5.25 μm are achieved over a PMA range of 76–89°. Such wide wavelength tunability is highly desired for applications such as molecular spectroscopy, environmental monitoring, etc.

4. Summary

We demonstrated, both theoretically and experimentally, a new efficient NLO material of 4H-SiC for tunable MIR generation by phase-matched DFG. It is revealed that 4H-SiC rather than 6H-SiC is appropriate to generate MIR radiation based on carefully measured refractive indices up to 5.00 μm. Broadband MIR radiation ranging from 3.90 to 5.60 μm is obtained experimentally in 4H-SiC. Much higher power is expected by optimizing the experimental design and improving the crystal quality. A 4H-SiC crystal is expected to be a promising NLO material in producing high-power MIR lasers in the future.

Acknowledgements. This work was partly supported by the National Natural Science Foundation of China under Grant Nos. 90922037, 51072222, and 51272276, the Ministry of Science and Technology of China (Grant No. 2011CB932700), the Chinese Academy of Sciences, and Beijing Nova Program (2011096).

Supporting information for this article is available free of charge under http://dx.doi.org/10.1002/lpor.201300068

Received: 13 May 2013, **Revised:** 20 June 2013,
Accepted: 20 June 2013

Published online: 19 July 2013

Key words: SiC, midinfrared, nonlinear optics, phase matching, difference-frequency generation.

References

[1] H. Preier, M. Bleicher, W. Riedel, and H. Maier, Appl. Phys. Lett. **28**, 669–671 (1976).
[2] J. Faist, F. Capasso, D. L. Sivco, C. Sirtori, A. L. Hutchinson, and A. Y. Cho, Science **264**, 553–556 (1994).
[3] Z. Shi, M. Tacke, A. Lambrecht, and H. Böttner, Appl. Phys. Lett. **66**, 2537–2539 (1995).
[4] Y. Yao, A. J. Hoffman, and C. F. Gmachl, Nature Photon. **6**, 432–439 (2012).
[5] D. Richter, A. Fried, and P. Weibring, Laser Photon. Rev. **3**, 343–354 (2009).
[6] E. Sorokin, S. Naumov, and I. T. Sorokina, IEEE J. Sel. Top. Quantum Electron. **11**, 690–712 (2005).
[7] C. F. Dewey and L. O. Hocker, Appl. Phys. Lett. **18**, 58–60 (1971).
[8] R. J. Seymour and F. Zernike, Appl. Phys. Lett. **29**, 705–707 (1976).
[9] R. C. Eckardt, Y. X. Fan, R. L. Byer, C. L. Marquardt, M. E. Storm, and L. Esterowitz, Appl. Phys. Lett. **49**, 608–610 (1986).
[10] K. L. Vodopyanov, V. G. Voevodin, A. I. Gribenyukov, and L. A. Kulevskii, Bull. Acad. Sci. USSR Phys. Ser. **49**, 146–149 (1985).
[11] K. L. Vodopyanov, L. A. Kulevskii, V. G. Voevodin, A. I. Gribenyukov, K. R. Allakhverdiev, and T. A. Kerimov, Opt. Commun. **83**, 322–326 (1991).
[12] Y. Furukawa, K. J. Kitamura, S. J. Takekawa, K. Niwa, and H. Hatano, Opt. Lett. **23**, 1892–1894 (1998).
[13] P. B. Phua, R. F. Wu, T. C. Chong, and B. X. Xu, Jpn. J. Appl. Phys. **36**, L1661–L1664 (1997).
[14] K. T. Zawilski, P. G. Schunemann, S. D. Setzler, and T. M. Pollak, J. Cryst. Growth **310**, 1891–1896 (2008).
[15] G. B. Abdullaev, K. R. Allakhverdiev, L. A. Kulevskii, A. M. Prokhorov, E. Y. Salaev, A. D. Savelev, and V. V. Smirnov, Sov. J. Quantum Electron. **5**, 665–668 (1975).
[16] N. Bloembergen, Appl. Opt. **12**, 661–664 (1972).
[17] B. C. Stuart, M. D. Feit, A. M. Rubenchik, B. W. Shore, and M. D. Perry, Phys. Rev. Lett. **74**, 2248–2251 (1995).
[18] A. Rosenfeld, M. Lorenz, R. Stoian, and D. Ashkenasi, Appl. Phys. A **69**, S373–S376 (1999).
[19] H. Morkoç, S. Strite, G. B. Gao, M. E. Lin, B. Sverdlov, and M. Burns, J. Appl. Phys. **76**, 1363–1398 (1994).
[20] V. E. Chelnokov and A. L. Syrkin, Mater. Sci. Eng. B **46**, 248–253 (1997).
[21] C. H. Carter, Jr., V. F. Tsvetkov, R. C. Glass, D. Henshall, M. Brady, St. G. Müller, O. Kordina, K. Irvine, J. A. Edmond, H.-S. Kong, R. Singh, S. T. Allen, and J. W. Palmour, Mater. Sci. Eng. B **61–62**, 1–8 (1999).
[22] G. Theodorou, G. Tsegas, and E. Kaxiras, J. Appl. Phys. **85**, 2179–2184 (1999).
[23] P. T. B. Shaffer, Appl. Opt. **10**, 1034–1036 (1971).
[24] S. Singh, J. R. Potopowicz, L. G. van Uitert, and S. H. Wemple, Appl. Phys. Lett. **19**, 53–56 (1971).
[25] N. W. Thibault, Am. Mineral. **29**, 327–362 (1944).
[26] B. Baugher and J. Goldstein, Opt. Mater. **23**, 519–528 (2003).
[27] S. Niedermeier, H. Schillinger, R. Sauerbrey, B. Adolph, and F. Bechstedt, Appl. Phys. Lett. **75**, 618–620 (1999).

[28] P. M. Lundquist, W. P. Lin, G. K. Wong, M. Razeghi, and J. B. Ketterson, Appl. Phys. Lett. **66**, 1883–1885 (1995).
[29] H. Sato, M. Abe, I. Shoji, J. Suda, and T. Kondo, J. Opt. Soc. Am. B **26**, 1892–1896 (2009).
[30] J. Chen, Z. H. Levine, and J. W. Wilkins, Phys. Rev. B **50**, 11514–11519 (1994).
[31] S. N. Rashkeev, W. R. L. Lambrecht, and B. Segall, Phys. Rev. B **57**, 9705–9715 (1998).
[32] B. Adolph and F. Bechstedt, Phys. Rev. B **62**, 1706–1712 (2000).
[33] I. J. Wu and G. Y. Guo, Phys. Rev. B **78**, 035447 (2008).
[34] "Laser and laser-related equipment-determination of laser-induced damage threshold of optical surface-part 1: 1-on-1 test" ISO Report No. 11254-1-2000.
[35] H. L. Sheng and G. M. Yang, Acta Metall. Sin. (China) **15**, 27–30 (1994).
[36] W. Zhang, H. Teng, C. X. Yun, X. Zhong, X. Hou, and Z. Y. Wei, Chin. Phys. Lett. **27**, 054211 (2010).
[37] See supplementary materials for detailed experimental results of refractive indices of 6H-SiC and 4H-SiC.
[38] D. A. Kleinman, Phys. Rev. **126**, 1977–1979 (1962).
[39] H. W. Xuan, Y. W. Zou, S. C. Wang, H. N. Han, Z. H. Wang, and Z. Y. Wei, Appl. Phys. B **108**, 571–575 (2012).
[40] F. Seifert, V. Petrov, and M. Woerner, Opt. Lett. **19**, 2009–2011 (1994).